Langmuir

Subscriber access provided by CASE WESTERN RESERVE UNIV

Article

Effect of Microstructure of Nitrogen-Doped Graphene on Oxygen Reduction Activity in Fuel Cells

Lipeng zhang, Jianbing Niu, Liming Dai, and Zhenhai Xia

Langmuir, **Just Accepted Manuscript** • DOI: 10.1021/la2043262 • Publication Date (Web): 10 Apr 2012

Downloaded from http://pubs.acs.org on April 13, 2012

Just Accepted

“Just Accepted” manuscripts have been peer-reviewed and accepted for publication. They are posted online prior to technical editing, formatting for publication and author proofing. The American Chemical Society provides “Just Accepted” as a free service to the research community to expedite the dissemination of scientific material as soon as possible after acceptance. “Just Accepted” manuscripts appear in full in PDF format accompanied by an HTML abstract. “Just Accepted” manuscripts have been fully peer reviewed, but should not be considered the official version of record. They are accessible to all readers and citable by the Digital Object Identifier (DOI®). “Just Accepted” is an optional service offered to authors. Therefore, the “Just Accepted” Web site may not include all articles that will be published in the journal. After a manuscript is technically edited and formatted, it will be removed from the “Just Accepted” Web site and published as an ASAP article. Note that technical editing may introduce minor changes to the manuscript text and/or graphics which could affect content, and all legal disclaimers and ethical guidelines that apply to the journal pertain. ACS cannot be held responsible for errors or consequences arising from the use of information contained in these “Just Accepted” manuscripts.

ACS Publications
High quality. High impact.

Langmuir is published by the American Chemical Society. 1155 Sixteenth Street N.W., Washington, DC 20036

Published by American Chemical Society. Copyright © American Chemical Society. However, no copyright claim is made to original U.S. Government works, or works produced by employees of any Commonwealth realm Crown government in the course of their duties.

Effect of Microstructure of Nitrogen-Doped Graphene on Oxygen Reduction Activity in Fuel Cells

Lipeng Zhang[a], Jianbing Niu[b], Liming Dai[c], Zhenhai Xia[b,*]

[a]Department of Mechanical Engineering, University of Akron, Akron, OH 44325, USA

[b]Department of Materials Science and Engineering, Department of Chemistry, University of North Texas, Denton, TX 76203, USA

[c]Department of Macromolecular Science and Engineering, Case Western Reserve University 10900 Euclid Avenue, Cleveland, Ohio 44106, USA

*Corresponding author: Email: Zhenhai.xia@unt.edu, Tel: 940-369-7673, Fax: 940-565-4824

ABSTRACT The development of fuel cells as clean-energy technologies is largely limited by the prohibitive cost of the noble-metal catalysts needed for catalyzing the oxygen reduction reaction (ORR) in fuel cells. A fundamental understanding of catalyst design principle that links material structures to the catalytic activity can accelerate the search for highly active and abundant non-metal catalysts to replace platinum. Here, we present a first-principles study of ORR on nitrogen-doped graphene in acidic environment. We demonstrate that the ORR activity primarily correlates to charge and spin densities of the graphene. The nitrogen doping and defects introduce high positive spin and/or charge densities that facilitate the ORR on graphene surface. The identified active sites are closely related to doping cluster size and dopant-defect interactions. Generally speaking, a large doping cluster size (the number of N atoms > 2) reduces the number of catalytic active sites per N atom. In combination with N clustering, Stone-Wales defects can strongly promote ORR. For four-electron transfer, the effective reversible potential ranges from 1.04~1.15 V/SHE, depending on the defects and cluster size. The catalytic properties of graphene could be optimized by introducing small N clusters in combination with material defects.

KEYWORDS: graphene · catalyst · oxygen reduction reaction · density functional theory

INTRODUCTION

Molecular oxygen reduction reaction (ORR) is a dominant process in many fields, such as energy conversion (fuel cells, metal-air batteries, etc.), corrosion or biology.[1-4] For fuel cells, cathodic ORR plays an essential role in producing electricity and is a major limiting factor on their performance.[5,6] Traditionally, platinum and its alloys [7-9] are used as electrocatalysts to promote the chemical reaction. However, platinum is expensive and susceptible to time-dependent drift [10]and CO poisoning.[2] These problems have been one of the major barriers in the development of fuel cells for large-scale commercial application. Thus, developing inexpensive electrocatalysts with high catalytic activities will accelerate the process of fuel cell commercialization.

Graphene and its derivatives represent a novel classic of two dimensional carbon nanomaterials. The 2D planar atomic-thick graphene exhibits better electronic properties due to its more freely electron transport when compared with other form of carbon while remains many unique properties including excellent electronic, mechanical and thermal properties. Previous studies have shown that graphene containing nitrogen atom has improved ORR activities, 3 times higher than platinum.[11] It is believed that the superior catalytic capabilities of these N-doped carbon nanomaterials are directly related to their unique nanostructure. Among the nitrogen-doped structures, pyrrolic and pyridinic nitrogen was reported to play an important role in the enhanced ORR activity in alkaline [11-14] and acidic [15,16] solutions. Stone-Wales defects have been predicted to alter the electronic properties (band structure and density of states) of graphene,[17-19] and in so doing modify its chemical reactivity toward adsorbates, and likely impact upon its catalytic properties. Although some theoretical work has been done on ORR pathway on N-doped graphene,[20-22] the role of materials structures, including N distribution and defects, played in ORR, remains unclear. Understanding how microstructure influences the catalytic behavior of the graphene will guide design and optimization of the electrocatalytic electrodes, and discovery of new catalysts.

In this study, we demonstrate via first-principles simulation that the ORR activities are directly correlated to material microstructure. The active catalytic sites are more likely to locate at the area with higher positive charge density and/or positive spin density. The number of dopants in cluster and Stone-Wales defects strongly affects the ORR on the N-doped graphene. This work motivates a direction for design of carbon nanostructured materials to improve their catalytic efficiency, and provides a theoretical framework for analysis of catalytic properties versus material structures.

METHODS

The ORR on nitrogen-doped graphene (G) in acidic fuel cells was studied using B3LYP hybrid density functional theory (DFT) through Gaussian 03 (Revision E.01; Gaussian, Inc., Wallingford, CT, 2004). The basis set for calculation is ground state and 6-31G (d, p). [23-26] Nitrogen atoms were incorporated into the armchair edge of the graphene to form pyridinic or pyrronic or mixed structures. Stone-Wales dislocations were also generated on the graphene. Stone-Wales defects are one of the important topological defects in sp^2-bonded carbon materials, playing a central role in the formation, transformation of carbon nanostructures.

We simulated the ORR processes starting with the first electron transformation, following the work on a Pt(111) by Wang et al. [5] Their work suggests that in an acidic environment, a decomposition is primarily driven by the chemisorption of hydroxyl, in line with Yeager's dissociative chemisorption proposal for the first step of ORR. [27] A unified mechanism for the first reduction step, which combines Damjanovic's [28] proton participation in the first electron reduction step and Yeager's dissociative chemisorption of O_2, is summarized as follows:

$$O_2 + H^+ \rightarrow OOH^+ \qquad (1)$$

$$OOH^+ + * + e^- \rightarrow *\text{-O-O-H} \qquad (2)$$

or

$$O_2 + * + e^- \rightarrow *\text{-O-O}^- \qquad (3)$$

$$*\text{-O-O}^- + H^+ \rightarrow *\text{-O-O-H} \qquad (4)$$

where asterisk represents a chemisorption site on graphene. In this step, we set OOH^+ or O_2 near the graphene plane at a distance of 3 Å, as schematically shown in Fig.1a. The optimized structures for OOH^+ or O_2 adsorption (ads) to graphene were obtained through structural optimization calculations. It is well-known that overall ORR can proceed by a two-step two-electron pathway with the formation of hydrogen peroxide or by a more efficient four-electron process to combine oxygen with electrons and protons directly in water. Hence, the ORR on graphene could follow either two-electron pathway or four-electron process, which will be examined in the simulation of subsequent electron transforming reactions.

The succeeding electron transforming reactions were simulated by keeping adding H atoms in the system. For each step, we obtained the optimized structure, and calculated the adsorption energy[29] (bond strength) for those molecules on the nitrogen-doped graphene. The adsorption energy is defined as the energy difference between the adsorption and the isolated systems while the bond strength is equal to the value of the adsorption energy but with opposite sign. Here, the energy of the isolated system refers to the sum of the energies of the fore-step adsorbed graphene and the individual isolated adsorbate molecules. So, negative adsorption energy indicates that the adsorbate molecule would be energetically favorable to be adducted to the surface of the nitrogen-doped graphene.

The reversible potential of each reaction step on the nitrogen doped graphene was also calculated following the procedure described by Roques and Anderson. [30] For an electrochemical reaction with reactants Ox and products Red:

$$\mathrm{Ox} + e^- (U^0) \rightarrow \mathrm{Red}, \qquad (5)$$

the relationship between the Gibbs free energy for a reduction reaction in aqueous (aq) solution and the reversible potential, U^0 is[30]

$$U^0 = \Delta G^0 / nF \qquad (6)$$

where ΔG^0 is the Gibbs free energy change of Eq. (5), n is the number of electrons involved in the reaction, and F is the Faraday constant. In this work, the Gibbs energy change is replaced by the reaction energy, E_r^0, plus constants. [30] So, Eq.(6) becomes

$$U^0 = E_r^0 / nF + U_1 + U_2 \qquad (7)$$

where the first constant U_1 represents $P\Delta V$ and $T\Delta S$ energy contributions, which depends on the solvation model used for the reactants and the products.[30] The second constant (U_2 = -4.6V) comes from the fact that the energy of an electron at 0 V on the electrochemical scale is -4.6 eV on the physical (vacuum) scale, [30] which is the one in which the quantum calculations take place. Eq. (7) is the reversible potential in aqueous solution. For the reaction on a catalyst surface,

$$(\mathrm{catalyst})\text{-}\mathrm{Ox} + e^- (U) \rightarrow (\mathrm{catalyst})\text{-}\mathrm{Red} \qquad (8)$$

the reversible potential U can be extrapolated from Eq. (7) assuming the constants U_1+U_2 unchanged:

$$U = U^0 + (E_r - E_r^0)/nF \qquad (9)$$

The change in reaction energy between Eq. (5) and Eq. (8), ΔE_r, is equal to the total adsorption energy of the reactants E_{ads} (Ox), minus the total adsorption energy of the products E_{ads} (Red): [31,32]

$$\begin{aligned}\Delta E_r &= E_r - E_r^0 \\ &= E_{(ads)}[Ox] - E_{(ads)}[\mathrm{Re}\,d]\end{aligned} \qquad (10)$$

So, the reversible potential on catalyst surface U is a function of adsorption energy and standard reversible reduction potentials U^0, for the reactions in bulk solutions: [31,32]

$$U = U^0 + \Delta E_{\mathrm{r}}/n\mathrm{F} \qquad (11)$$

where U^0 is the standard solution-phase potential. Thus, if we know the reversible potential in an aqueous solution of a redox reaction U^0 (from experimental or theoretical investigations), we will be able to calculate the reversible potential on a specific catalyst surface U just by the knowledge of the adsorption energies of each species involved in the reaction.

It should be noticed that in the ORR we study here, OOH^+ and H^+ exist in aqueous solution but the total adsorption energy of the chemical species are calculated using OOH, and H. This is reasonable because the effect of charge has been considered by using the known reversible potential in an aqueous solution of a redox reaction U^0. The predictions are very close to the experimental results. [30-32] Nevertheless, care should be taken when using this method to calculate the reversible potentials. For example, the coverage rate of OH (ads) and OOH (ads) on graphene may be considered in order to get more accurate results, in particular, when comparison is made between different pathways and concerning the existence of species like OOH in solution (and not near the surface) or OH in solution.

RESULTS AND DISCUSSION

Catalytic pathways of ORR on N-doped graphene

We first studied catalytic pathways of graphene with two nitrogen atoms incorporated into the hexagon and the pentagon of the graphitic sheet with two combined Stone-Wales defects, as shown in Figure 1. Such structures are pyridinic and pyrrolic mixed type of nitrogen atoms in the nitrogen-doped graphene. As mentioned above, there are two possible reaction pathways in the first electron transfer: i) intermediate molecule OOH^+ adsorption, and ii) direct O_2 adsorption. We first simulated the ORR processes beginning with the first electron transformation in an acidic environment, in which process an intermediate molecule OOH^+ has been formed. Simulation shows that the both OOH^+ and OOH molecule far from the graphene (~3 Å) can adsorb on the graphene at carbon atom #16, as shown Fig.1(b). This result indicates that there is no energy barrier in the reaction. After adsorption, the graphene plane distorted into "saddle shape" warped surface while the carbon atom attached to the oxygen raises out of the plane to form a tetrahedral structure.

The O_2 adsorption on the N-doped graphene was simulated with the same procedure as OOH adsorption. O_2 cannot adsorb on the graphene at carbon atom #16, even when O_2 molecule is put in the range of bonding formation. However, O_2 can adsorb on the same site of the negatively charged graphene. The adsorbed O_2 can further interact with an H^+ to form an adsorbed OOH. Therefore, the surface charge promotes the adsorption of O_2. However, the O_2 adsorption energy is -0.7eV, over 10 times smaller than that for OOH^+ adsorption (-11.26 eV). This implies that OOH^+ adsorption is a more favorable reaction in the first electron transfer.

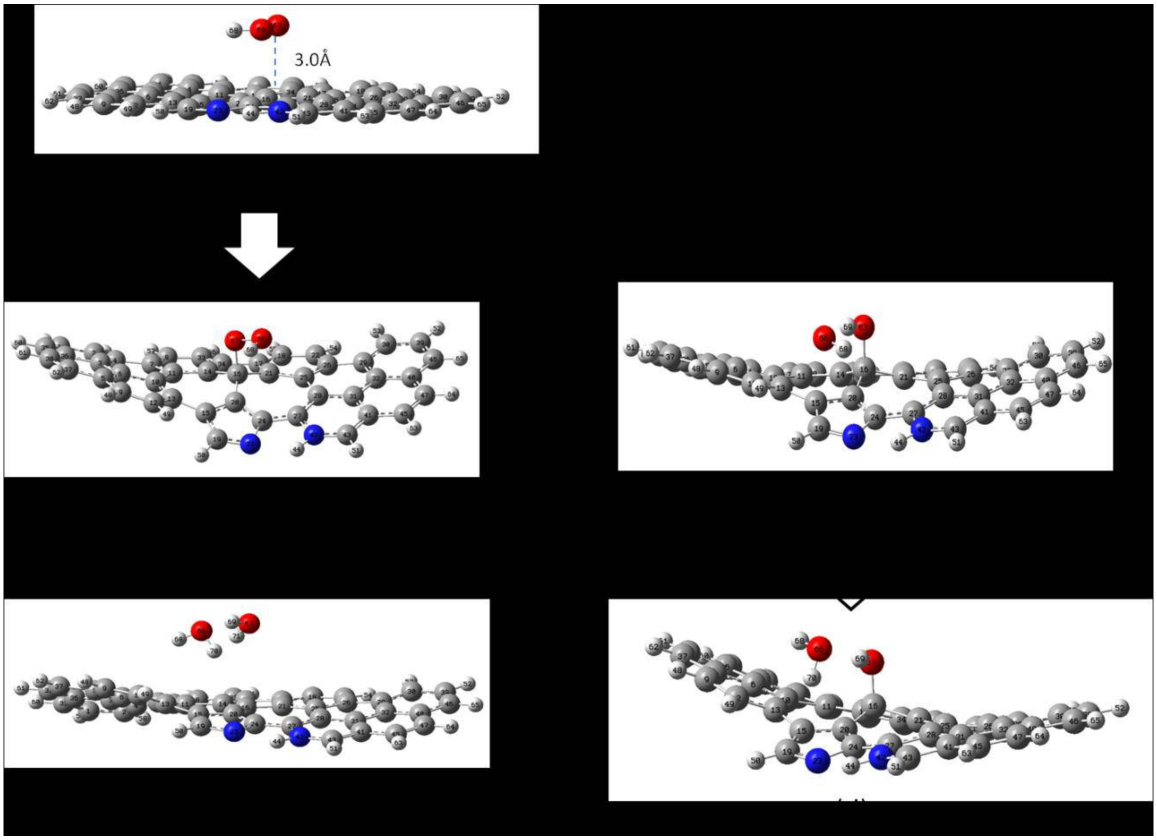

Figure 1. Optimized structure of each electron transformation in oxygen reduction reaction: (a) Initial position of OOH from nitrogen doped graphene, (b) OOH adsorbs on the graphene, (c) O-O bond is broken, (d) One water molecule is generated, and (e) C-O bond is broken, the second water molecule is generated. Grey, blue, red and small white balls represent carbon, nitrogen, oxygen and hydrogen atoms, respectively.

When adding an H atom near the oxygen atom that attaches to the graphene, a bond is formed between the oxygen and the hydrogen atoms. At the same time, the O-O bond is broken, resulting in the formation of a hydroxide molecule OH, as shown in Figure 1c. During this process, the distance between the two O atoms changed from an initial value of 1.45 Å to a value of 2.72 Å. The dissociated OH moves away from the graphene plane, while the other dissociated OH is still bonding to the graphene. This is a typical four electron reaction because the O-O bond breaks during the reaction. [33, 34]

After adding two more H atoms to the O atoms in the reaction system, two water molecules are formed and completely departed from the graphene (Figure 1d, and e). The third and fourth electrons were then transformed in the oxygen reduction reaction. Finally, after the removal of the water molecules, the "saddle-shaped" graphene recovers to its original shape and is ready for next reaction cycle.

The above chemical reactions, adsorption energy difference between reactants and products, standard reversible potential and reversible potential on the catalyst surface are listed in Table 1. For each step of electron transformation, the reversible potential is positive, suggesting that the system moves to a more stable state during the reactions. So, the four electron reaction can spontaneously take place on this nitrogen-doped graphene. Of all the reaction steps, OOH molecular adsorption on the graphene (Reaction 1) is one of the most important steps for the catalytic reaction of oxygen reduction because it determine whether a nitrogen-doped graphene electrode has catalytic activity or not. The O-O bond break in Reaction (2) is another key necessary step for the four electron reaction. The reversible potential for overall ORR is U_s^0 = 1.228 V(SHE), which is consistent with standard reversible potential of ORR. [35,36] It should be noted that during the ORR process, Carbon #16 is not the only one active site for the ORR. We found that OOH molecule is also able to adsorb to Carbon #22 and #24 and the succeeding reactions can occur spontaneously.

Table 1. Adsorption energy difference and reversible potentials of each ORR step on the graphene with two doped nitrogen atoms and two Stone-Wales defects.

Reaction order	Chemical Reaction	Adsorption energy difference ΔE_r (eV)	Reversible potential U^0 (V/SHE) †	Reversible potential U (V/SHE)
1	$O_2+H^++e^-\rightarrow$*OOH	1.170	-0.046	1.120
2	*OOH$+H^++e^-\rightarrow$*OH+OH	1.150	-0.664	0.480
3	$OH+H^++e^-\rightarrow H_2O$	0.0	2.813	2.813
4	*OH$+H^++e^-\rightarrow H_2O$	-2.320	2.813	0.493
Overall	$O_2+4H^++4e^-\rightarrow 2H_2O$	0.00	1.229	1.228

† Ref.31.

From quantum mechanics, the nitrogen doping creates an electron acceptor state in the conduction band near the Fermi level.[37,38] The electron-accepting ability of the nitrogen atom creates net positive charge on adjacent carbon atoms in the graphene plane, resulting in redistribution of spin density and charge density around the nitrogen atoms, which will influence the OOH adsorption and further O-O bond breakage. It was shown that the adsorption bond strengths of adsorbate radicals, H and OOH, exhibit a correlation with the spin density. [29] So, spin density may be regarded as a factor determining positional selectivity of radical adsorption while charge density determines the attractive force between charged atoms. It is expected that the active catalytic sites for OOH adsorption should be those atoms with high spin density and/or high positive charge. We have calculated the spin density and charge density for a given N-doped structure. Figure 2 shows the typical spin density and charge density distributions on the nitrogen doped graphene. For an N dopant, the atoms with high charge density are always those bonded to the nitrogen atoms while those with high spin density are the second or third neighboring carbon atoms. Most identified active sites are those carbon atoms with high charge or spin density or high value of combination of charge and spin. For example, for the graphene with two doped nitrogen atoms and Stone-Wales defects, carbon #27 and #24 possess the highest and second highest atomic charge density (Figure 2a) while Carbon #16 has the highest spin density (Figure 2b). These atoms are the catalytic active points identified for the ORR.

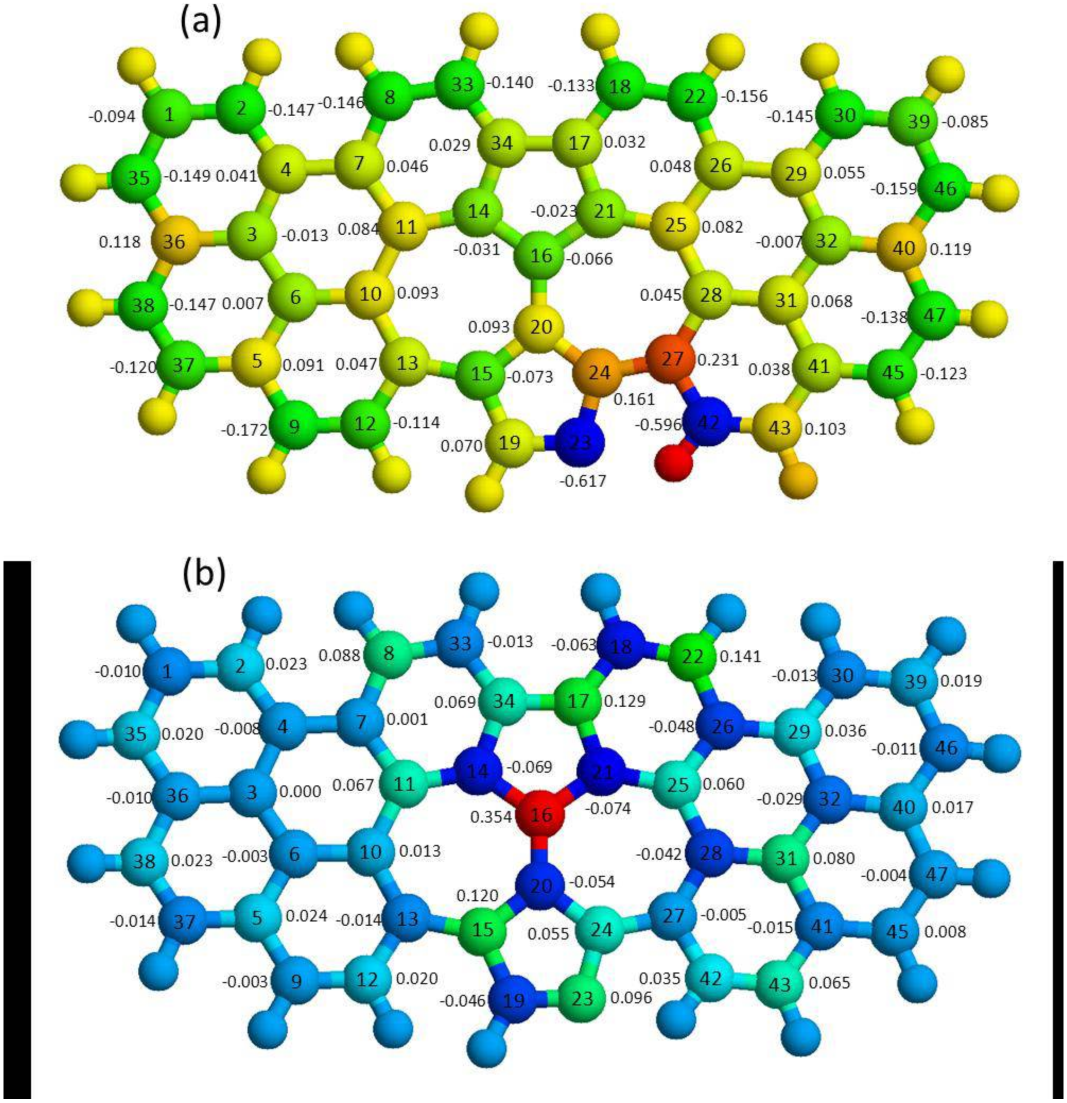

Figure 2. (a) Atomic charge density and (b) Spin density distribution on the nitrogen-doped graphene with Stone-Wales defects.

As mentioned above, OOH adsorption on graphene represents one of the most important steps for ORR. The adsorption energies of OOH may be sensitive to atomic charge density and spin density of the active sites. We have calculated the charge and spin densities of active sites on several kinds of nitrogen doped graphene structure, in which the number of doped nitrogen atoms increases from one to four in cluster. Figure 3 shows the adsorption energy as a function of atomic charge density *e* and spin density *s*. For atomic charge density *e*= -0.087 ~ +0.085, and *e* = +0.205 ~ +0.263, the adsorption energy increases nearly linearly with increasing the spin density (Figure 3a), which is consistent with the results obtained by Sidik and Anderson.[29] On the other hand, the adsorption energy also increases with increasing the atomic charge density but with large scattering (Figure 3b). It should be noted that for the case of no spin density, only those atoms with relatively high charge density can act as a catalytic site, but these sites with high charge density usually lead to much higher adsorption energy. Therefore, any approaches that increase the spin or charge density of carbon atoms will facilitate the ORR on graphene surface.

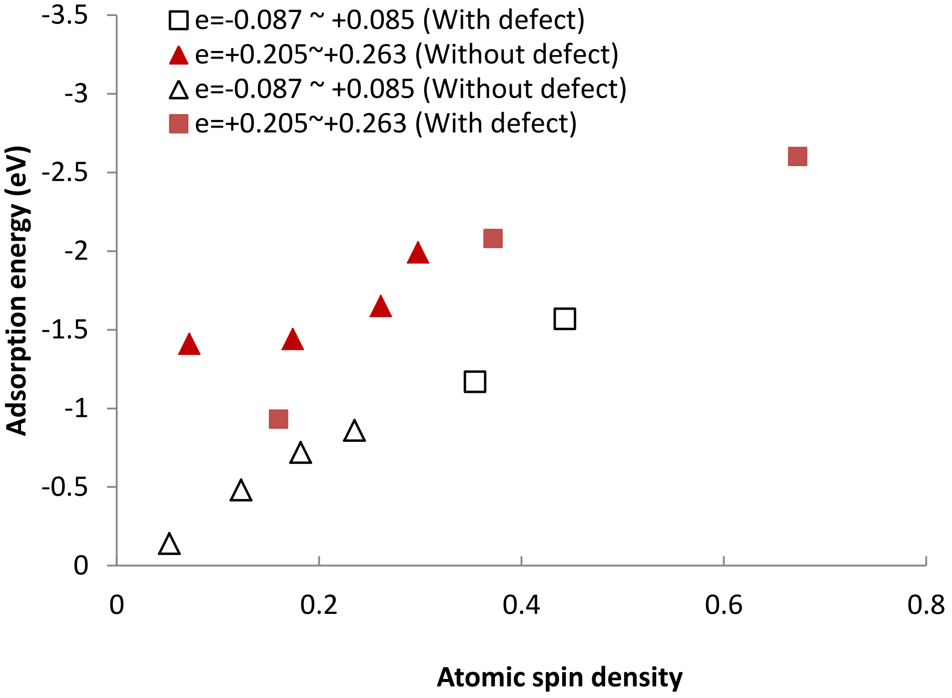

(a)

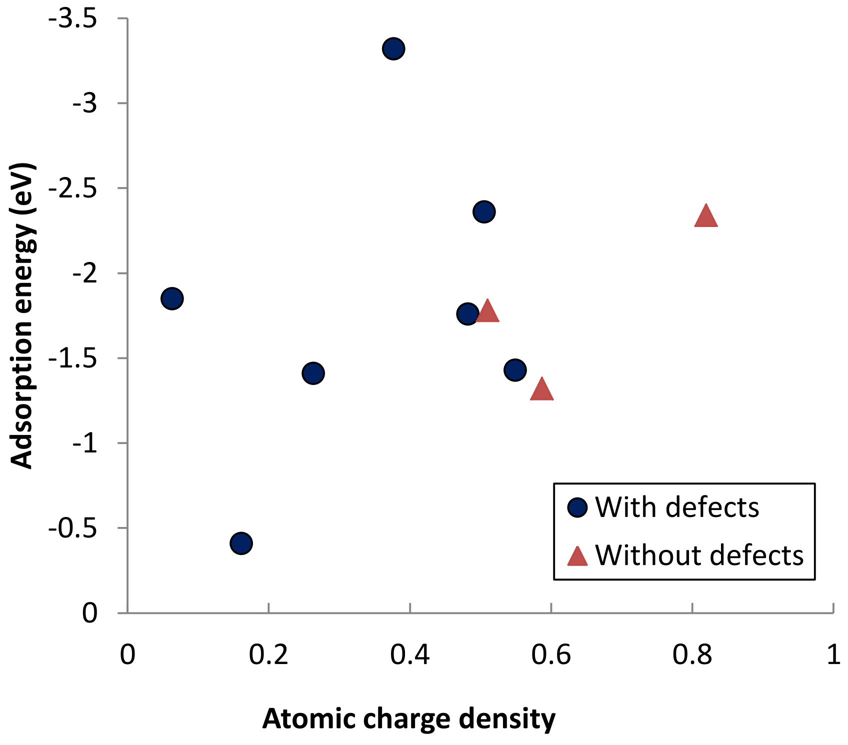

(b)

Figure 3. The adsorption energy of OOH on graphene as a function of (a) Spin density for atomic charge e= -0.087 ~ +0.085, and e = +0.205 ~ +0.263, and (b) Atomic charge density for s= -0.036 ~ +0.0072. The adsorption energy is calculated from Reaction (15) in the absence of charge.

The above energy calculation was performed without considering the presence of charge. We have calculated the adsorption energy of OOH^+ adsorbs on the graphene that carries a negative charge. As expected, the charge on graphene does influence adsorption; however, the reaction energy is closely correlated with that in the absence of charge. For example, for OOH^+ adsorption reaction on the graphene (G) shown in Figure 1a,

$$G(e^-) + OOH^+ \rightarrow G\text{-}OOH, \qquad (12)$$

the reaction energy is -11.25 eV. It consists of two elementary reactions:

$$G(e^-) \rightarrow G + e^- \qquad (13)$$

$$OOH^{+} + e^{-} \rightarrow OOH \qquad (14)$$

with the reaction energies of 1.80 eV (graphene electron affinity) and -11.89 eV (OOH ionization potential), respectively. For the same reaction without considering the charge,

$$G + OOH \rightarrow G\text{-}OOH \qquad (15)$$

with a reaction energy of -1.16 eV. Thus, the reaction energy of Reaction (12) should be the energy sum of Reactions (13) ~ (15). Since Reactions (13) and (14) is the deionization process of OOH and graphene, their reaction energy should be constant for a given graphene structure under the standard condition. Thus, the adsorption energy calculated without considering the charge E_1 is equal to that in the presence of charge E_2, plus a constant c: $E_1 = E_2 + c$.

As externally introduced charges may influence the charge and spin density on graphene and further ORR process, we have examined the charge and spin density distribution on N-doped graphene in the presence of an additional negative charge. It turns out that the additional charge does not influence the charge distribution on graphene (slight variation in magnitude). Thus, the additional charge does not affect the ORR mechanisms on the graphene. On the other hand, the spin density change is complicated in the presence of charges. When one additional negative charge is introduced onto the graphene, the spin density disappears. When two additional negative charges are introduced, the spin density redistributes, but the overall distribution is similar to those before the charge is introduced, i.e. there is always one carbon atom with a maximum spin density of ~0.35-0.4, in adjacent to the nitrogen atoms. In this case, the catalytic ability should remain similar even when additional charges are introduced. More work is needed to understand the radical reactions and the effect of spin density on graphene.

Effect of nitrogen doping structures and defects on the catalytic behavior

Apart from the structures with two nitrogen doping atoms, we have examined the catalytic activities of various graphene structures with a cluster of dopants and defects (Fig.4). Note that N atoms are separated by 2-3 crystal lattices (~2-3 Å) such that there is no N-N bond in the clusters. Recent DFT calculation showed that the formation of N-N bond in graphene is energetically unfavorable, and the probability of having two doped N atoms at neighboring sites is quite low.[39] More recently, Scanning Tunnel Microscopy (STM) direct imaging on N-doped graphene revealed that most N atoms exist either isolated or in cluster in which N atoms are separated in several lattices.[40] We also calculated the energies of all these optimization structures of nitrogen doped graphene with N-N bond and those with N atoms separated. The energy of former is higher than that of the later. So all the clusters generated in this study are energetically favorable.

The reaction energy and reversible potential for each reaction step of ORR on these nitrogen-doped graphene were calculated. Figure 5 shows the reversible potential for each reaction step of ORR as a function of the number of N doping atoms. OOH molecule cannot adsorb on graphene without N doping, indicating that the N doping is a key to graphene as an ORR catalyst. For the graphene without defects, with increasing the number of nitrogen atoms in the cluster, the reversible potential of O-O bond dissociation rapidly increases while the potential of water forming slightly reduces, but the potential for *OOH adsorption does not change too much. Therefore, the N clustering can significantly promote the O-O bond dissociation reaction. For the graphene with defects, the reversible potential changes quite differently compared to N doping alone. When the size of N clusters increases, the reversible potential of O-O bond dissociation quickly reduces to a value around the standard reversible potential (1.228V, dot lines in Figure 5), whereas the potential for water forming quickly increases to the same range. The potential for *OOH adsorption varies slightly around the standard value. So, in the presence of defects, the N clustering makes the reversible potentials of each reaction step closer to the ideal reversible potential. Relatively equal potentials in each reaction step may increase the reaction rate in ORR. [29] These results suggest that ORR occurs more easily on the nitrogen doping clustering with defects than the single nitrogen doping. Although the defects alone do not have catalytic capability, the combination of the N cluster and defects can strongly facilitate the ORR on graphene.

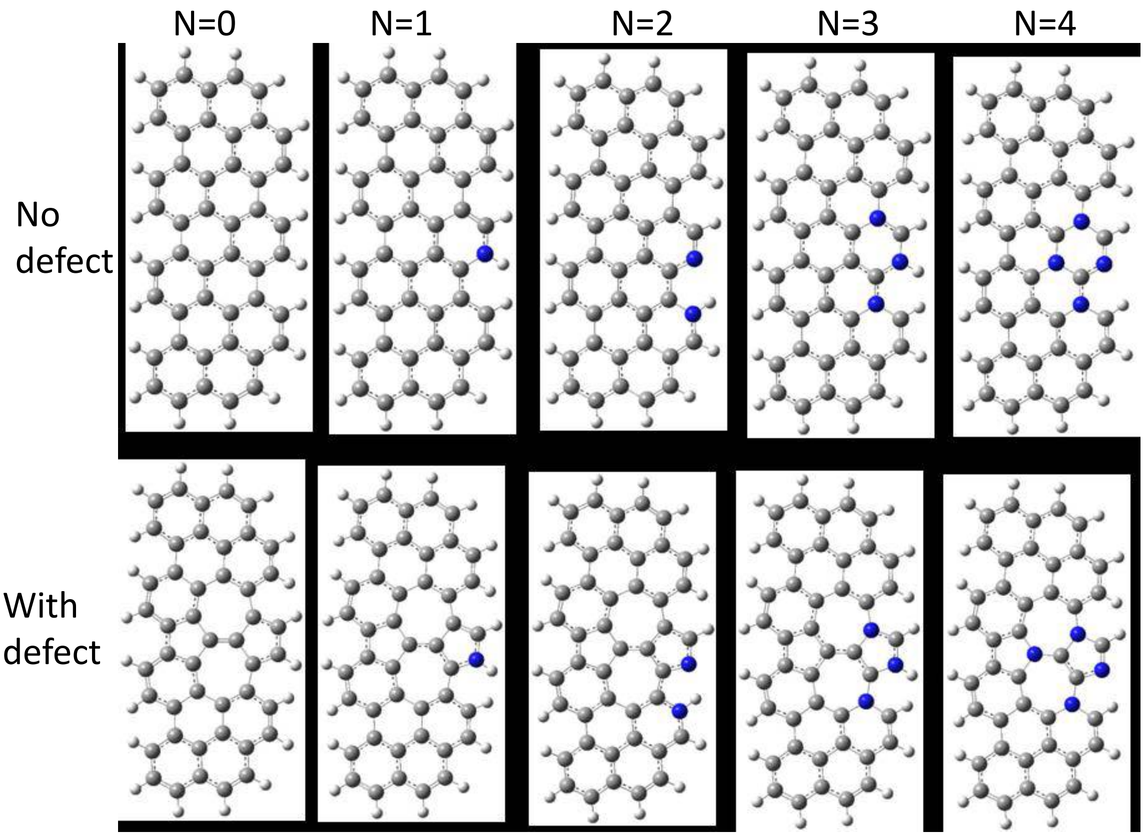

Figure 4. The graphene structures with a number of dopants and defects. N= the number of nitrogen dopants. Grey, blue, and small white balls represent carbon, nitrogen, and hydrogen atoms, respectively. The structures in the first row contain no defects while the structures in the second row have.

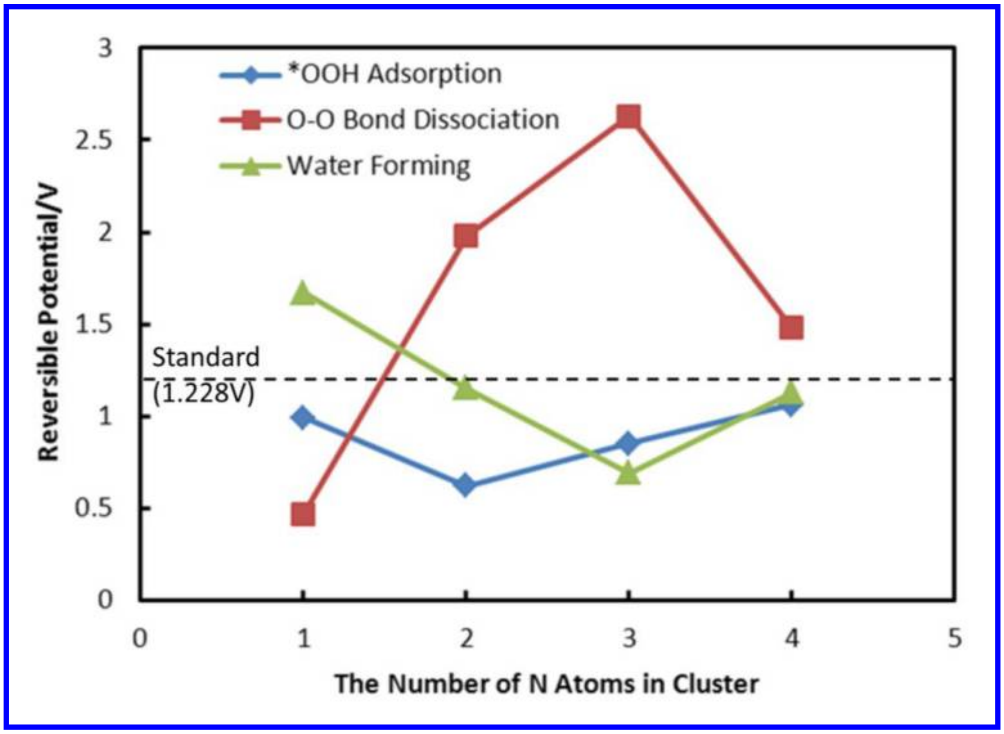

(a)

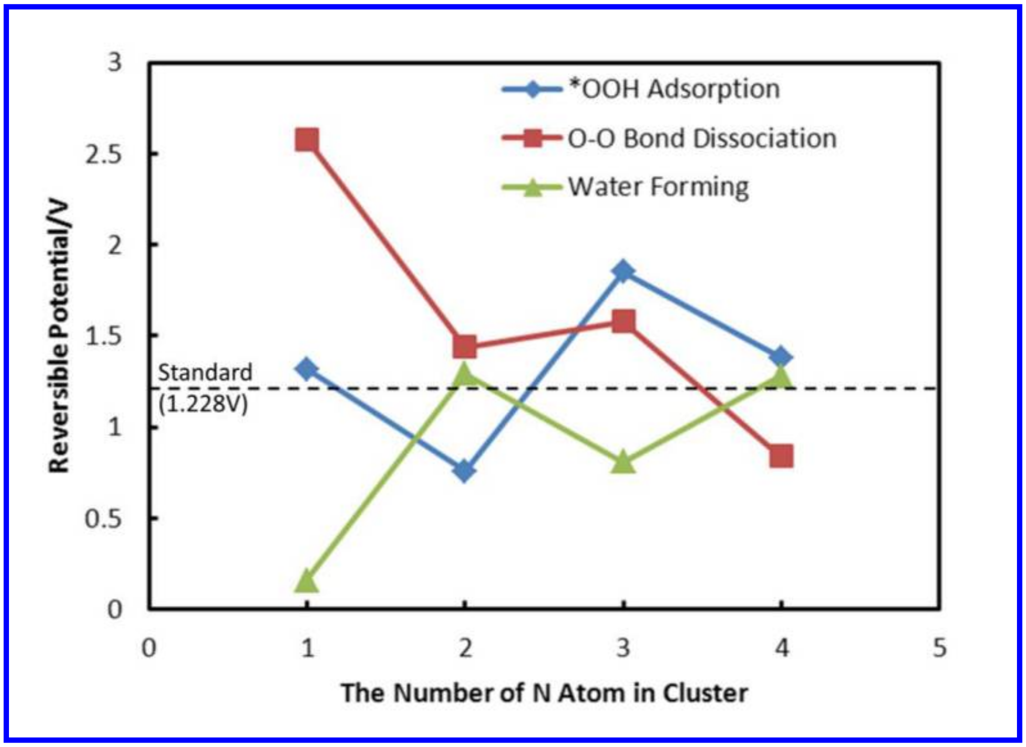

(b)

Figure 5. The reversible potentials of ORR versus N cluster size for the graphene (a) without defects, and (b) with defects. Dot lines represent standard reversible potential (1.228 V).

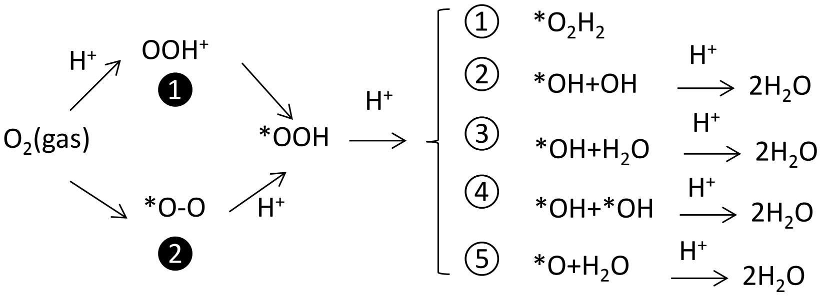

Figure 6. Reaction scheme of ORR on N-graphene in acidic solution, where ❶ presents an intermediate OOH adsorption mechanism and ❷ a direst O_2 adsorption mechanism, and ① ~ ⑤ represents 5 reaction pathways after OOH adsorption.

The N cluster and defects also influence the reaction pathway. In addition to the reaction path listed in Table 1, different reaction routes and catalytic behaviors were observed for multiple-doping graphene. The identified reaction pathways include two-electron transfer (path ① in Figure 6) and four-electron transfer (Paths ② -⑤). Path ① is a typical two-electron transfer reaction while all other reaction paths identified are four-electron transfer reaction. The reversible potential for Path ① is 0.685 V, which is consistent with the results from the literature. [29] The two-electron process usually is much less efficient than four-electron one.[12] For Path ③, the introduction of a hydrogen results in O-O bond breaking and formation of two OH molecules. One adsorbs on the same site as the OOH on graphene while the other combines with H that bonds to a nitrogen atom to directly form a water molecule. Finally, the adsorbed OH combines with H to form a water molecule. The overall reaction reversible potential is 1.228 V. Path ④ is similar to that listed in Table 1, but here both OH molecules adsorb on graphene. In the last path (Path ⑤), O-O bond breaking generates an adsorbed O and a water molecule. H further reacts with the adsorbed O to form water. The overall reversible potential is also 1.228 V, which is equal to the standard reversible potential U^0 of oxygen and hydrogen redox reaction. This value corresponds to the standard Gibbs energy of reaction, $\Delta G^0 = 4.916$ eV, and is the maximum energy available to do electrical work.

The above reversible potentials were calculated under the assumption that all the Gibbs free energy is converted into electric work. However, the experimentally observed onset potential for O_2 reduction to water over nitrogen-doped graphene and carbon nanotube is usually much smaller than the standard reversible potential 1.228 V. This overpotential is caused by the exergonicity of OOH (ads) dissociation step.[35] In principle, any exergonic reaction that does not include the transfer of an electron during the course of the overall reaction will cause the overpotential, even if all of the electron transfer steps are activationless. In this study, the OOH (ads) dissociation reaction occurs on the N-doped graphene in four electron transfer ORR. For Path ②, Reaction (2) in Table 1 can be separated into two sub-reactions: $^*OOH \rightarrow {}^*O + OH$ and $^*O + e^- + H^+ \rightarrow {}^*OH$. Similarly, O-O bond dissociation reaction in

Path ③ contains two sub-reactions: $*OOH \rightarrow *O + OH$ and $*O + OH + 2e^- + 2H^+ \rightarrow *OH + H_2O$ while in Path ④ the dissociation reaction is: $*OOH \rightarrow *O + OH$ and $*O + OH + e^- + H^+ \rightarrow *OH + *OH$. For Path ⑤ the dissociation reaction is: $*OOH \rightarrow *O + OH$ and $*O + OH + e^- + H^+ \rightarrow *O + H_2O$. In the ideal case, this dissociation reaction will be energonic neutral. In the nonideal case (like the reaction on catalytic surfaces), when the reaction is exergonic, free energy $\Delta G'$ is lost. Thus, $\Delta G'$ is not available for electrical work and should be subtracted from ΔG^0. The Gibbs energy available for electrical work is:

$$\Delta G_w = \Delta G^0 - \Delta G' \qquad (16)$$

Similar to the treatment in Eq. (6), $\Delta G'$ is replaced by the reaction energy E_{ex} for the exergonic reaction. Thus, the effective reversible potential U_{eff} can be written as

$$U_{eff} = - \Delta G^0/(nF)+E_{ex}/(nF) \qquad (17)$$

We calculated the lost Gibbs free energy $\Delta G'$ of exergonic reaction ($*OOH \rightarrow *O + OH$) included in Paths ② ~ ⑤, yielding 0.56 eV, 0.63 eV, 0.30 eV and 0.74 eV, respectively. So, the effective reversible potential U_{eff} of Path ①, Path ③, Path ④ and Path ⑤ is 1.09 V, 1.07 V 1.15 V, and 1.04 V respectively.

We also found incomplete reaction paths at some active sites, mostly on the graphene with large N clusters. For example, after OOH adsorption, $O_2 + H^+ + e^- \rightarrow *OOH$, ($U$=2.55 V/SHE) and O-O disassociation, $*OOH + 2H^+ + e^- \rightarrow *OH + H_2O$, ($U$=1.83 V/SHE), the reversible potential of the following steps, $*OH + H^+ + e^- \rightarrow H_2O$ is -1.13 V/SHE, which cannot occur spontaneously. In all these incomplete paths, either OOH adsorption or O-O disassociation potential or both are too high. As a result, the next reactions are suppressed.

The number of active sites and effective reversible potential against the size of N clusters are summarized in Table 2. Overall, with increasing the size of N cluster, the number of active sites per nitrogen atom first increases to a maximum value at double N cluster, and then reduces linearly. In the presence of defects, more active sites are created when N dopants exist in cluster. This effect can be attributed to the interaction between the defect and dopants. Considering the fact that the defects make the reversible potentials closer to the ideal value (1.228V) (Figure 5b) if N exists in the form of clustering, a small cluster (ideally two N) combining with defects would maximize the catalytic active sites available for ORR. Interestingly, recent study shows that most N dopants exist in single N or double N cluster on single-layered graphene.[40]

Table2. The number of active sites and effective reversible potential for nitrogen-doped graphene.

	The number of N atoms in cluster	**0**	**1**	**2**	**3**	**4**
No defect	The number of active sites	0	1	3	2	1
	Effective Reversible potential V/SHE	-	1.04	1.07~1.15	1.07	1.15
With defect	The number of active sites	0	1	3	2	3
	Effective Reversible potential V/SHE	-	1.04	1.15	1.07~1.15	1.15

Although it is still a challenge to experimentally realize the doping of graphene or carbon nanotubes (CNTs) with N clusters, the general trends demonstrated in this study consist well with experimental observations. For instance, a reversible (turn-on) potential around 1 V (*vs.* SHE) was observed for N-doped CNTs in an acidic medium. [41] In consistent also with the present study, the overpotential for a two-electron ORR process has been previously observed to be about half that of its four-electron counterpart catalyzed by N-doped graphene and carbon nanotubes.[11,12] Furthermore, our preliminary results indicate that the ORR catalytic activities of N-doped carbon nanotubes and graphene increase with the acid-oxidation to introduce structure defects. Doping of graphene with elements (S, Cl) [42] of similar electronegativities as that of nitrogen could also impart the ORR activities, presumably due to the doping-induced spin redistribution.

To further examine the effect of the doping and defects on the catalytic behavior of graphene, we calculated energy separation between the highest occupied molecular orbital (HOMO) and lowest unoccupied molecular orbital (LUMO), which can be used as a simple indicator of kinetic stability. The smaller energy gap means that the state of the graphene is energetically favorable to add electrons to a high-lying LUMO, to extract electrons from a low-lying HOMO, and so to form the activated complex of any potential reaction.[43] The HOMO-LUMO gaps of graphene with and without defects versus the number of nitrogen atoms in cluster are shown in Figure 7. In the absence of defects, the incorporation of one or two nitrogen atoms into the graphene lattice reduces HOMO-LUMO gap by a factor of 2.3 compared to perfect graphene, but with further increasing N cluster size (3~4N), the gaps increase to a level of ~1.7 eV from 1.1 eV. This trend is consistent with the results listed in Table 2, where the number of active sites reduces with increasing the cluster size. In the presence of Stone-Wales defects, the HOMO-LUMO energy gap is much lower than the perfect graphene. The insensitivity of the gap to the introduction of N dopants suggests that the chemical reactivity of the graphene is controlled by the defects. As a result, all the Stone-Wales defective graphene has relatively high chemical reactivity. As shown in Table 2, the number of active sites on graphene with defects is more than that on the graphene without the defects. In addition to increasing the number of active sites, defects can promote some catalytic reactions, i.e., the adsorption and O-O bond breaking reactions (Figure 5). However, in the case of large N cluster, the combination of N cluster and defects can sometimes over-promotes these reactions with a consequence of blocking the following reactions (i.e., water formation). As discussed above, the presence of N dopants generated active sites that have high adsorption energy (e.g. OH on graphene). However, the bonds may be too strong to break in the following reactions. Consequently, the following catalytic reactions cannot occur spontaneously. Thus, to optimize the catalytic performance, materials structures should be controlled to have small N doping clusters in combination with material defects.

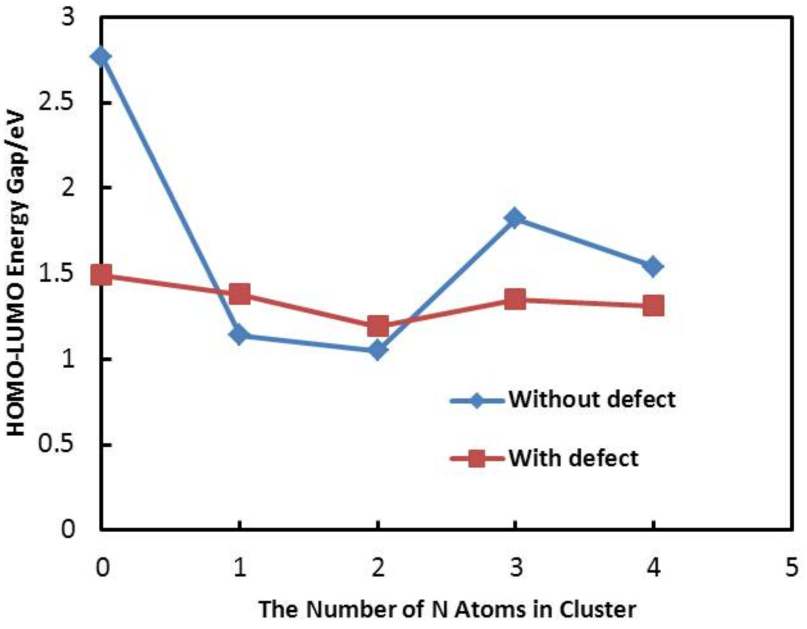

Figure 7. HOMO-LUMO energy gap as a function of the number of nitrogen doped atoms in cluster with and without Stone-Wales defects.

CONCLUSIONS

DFT method was used to study the effect of nitrogen-doping and Stone-Wales defects on ORR in fuel cells. Simulation results show that dopant-induced redistribution of spin density and charge density on the graphene strongly affect the formation of the intermediate molecules in ORR, including OOH, or O_2 adsorption, O-O bond break and water formation. With increasing the number of nitrogen dopants from one to four in cluster, the number of active sites per doping atom reaches to maximum at N=2 and then reduce, indicating that catalytic ability of nitrogen in larger cluster is weaker than that of single nitrogen or small cluster in terms of the number of catalytic sites available. The defects enhance the catalytic capability of the graphene by changing the HOMO-LUMO energy gap and reaction pathways. For four-electron transfer, the predicted effective reversible potential for N-doped graphene is in the range of 1.04~1.15V/SHE with an average value of 1.10V/SHE, which is consistent with the experimental results. Engineering materials structures can promote catalytic capability of graphene by introducing small N clusters in combination with materials defects

ACKNOWLEDGMENT

The authors acknowledge the support from NSF (CMMI-1000768, and CMMI-0825990) and AFOSR MURI (FA9550-12-1-0037).

REFERENCES

(1) Steele, B. C. H.; Heinzel, A.; Materials for fuel-cell technologies; *Nature* **2011**, *414*, 345.

(2) Winther-Jensen, B.; Winther-Jensen, O.; Forsyth, M; High rates of oxygen reduction over a vapor phase-polymerized PEDOT electrode; *Science* **2008**, *321*,671.

(3) Khelashvili, G.; Behrens, S.; Vetter, C.; Hinsch, A.; Kern, R.; Skupien,K.; Dinjus, E.; Bonnemann, H.; Catalytic platinum layers for dye solar cells: A comparative study; *Thin Solid Films* **2006**, *511*, 342.

(4) Goux ,A.; Pauporté, T.; Lincot, D.; Oxygen reduction reaction on electrodeposited zinc oxide electrodes in KCl solution at 70 ºC; *Electrochimica Acta* **2006**, *51*, 3168

(5) Wang, Y.; Balbuena, P.B.; Ab initio molecular dynamics simulations of the oxygen reduction reaction on a Pt(111) surface in the presence of hydrated hydronium $(H_3O)^+(H_2O)_2$: Direct or series pathway?; *J. Phys. Chem. B* **2005**, *109*, 14896.

(6) Basu, S.; Ed., *Recent Trends in Fuel Cell Science and Technology* Springer New York, 2007.

(7) Che, G.; Lakshmi, B. B.; Fisher, E.R.; Martin, C.R.; Carbon nanotube membranes for electrochemical energy storage and production; *Nature* **1998** *393*, 346.

(8) Gong, K.; Yu, P.; Su, L.; Xiong, S.; Mao, L.; Polymer-assisted synthesis of manganese dioxide/carbon nanotube nanocomposite with excellent electrocatalytic activity toward reduction of oxygen; *J. Phys.Chem. C* **2007**, *111*, 1882.

(9) Kongkanand, A.; Kuwabata, S.; Girishkumar, G.; Kamat, P.; Single-wall carbon nanotubes supported platinum nanoparticles with improved electrocatalytic activity for oxygen reduction reaction;

Langmuir **2006**, *22*, 2392.

(10) Collman, J. P.; Devaraj, N. K.; Decreau, R. A.; Yang, Y.; A cytochrome c oxidase model catalyzes oxygen to water reduction under rate-limiting electron flux; *Science* **2007**, *315*, 1565.

(11) Qu, L.; Liu,Y.; Baek, J. B.; Dai, L.; Nitrogen-doped graphene as efficient metal-free electrocatalyst for oxygen reduction in fuel cell; *ACS Nano*, **2010**, *4*, 1321.

(12) Gong, K.; Du, F.; Xia, Z.; Dustock, M.; Dai, L.; Nitrogen-doped carbon nanotube arrays with high electrovatalytic activity for oxygen reduction; *Science* **2009**, 323.

(13) Luo, Z.; Lim, S.; Tian, Z.; Shang, J.; Lai, L.; MacDonald, B.; Pyridinic N doped graphene: synthesis, electronic structure, and eletrocatalytic property; *J. Mater. Chem.* **2011**, *21,* 8038.

(14) Shao, Y. ; Zhang, S.; Engelhard, M. H.; Li, G.; Shao, G.; Wang,Y.; Nitrogen-doped graphene and its electrochemical applications; *J. Mater. Chem*. **2010**, *20*, 7491.

(15) Lee, K.; Lee, J.; Ahn, B.; Woo, S.; Electrochemical oxygen reduction on nitrogen doped graphene sheets in acid media; *Electrochemistry Communications* **2010**, *12,* 1052.

(16) Wang, P.; Wang, Z.; Jia, L.; Xiao, Z.; Origin of the catalytic activity of graphite nitride for the electrochemical reduction of oxygen: geometric factors vs. electronic factors; *Phys. Chem. Chem. Phys.* **2009**, *11*, 2730.

(17) Meyer, J. C.; Kisielowski, C.; Erni,R.; Rossell, M. D.; Crommie, M.F.; Zettl, A.; Direct imaging of lattice atoms and topological defects in graphene membranes; *Nano Letters* **2008**, 8, 3582.

(18) Boukhvalov, D.W.; Katsnelson, M.I.; Chemical functionalization of graphene with defects; *Nano Letters* **2008**, 8, 4373.

(19) Banhart, F.; Kotakoski, J.; Krasheninnikov, A. V.; Structural defects in graphene; *ACS Nano* **2011**, 5, 26.

(20) Zhang,L.; Xia, Z.; Mechanism of oxygen reduction reaction on nitrogen-doped graphene for fuel cells; *J. Phys. Chem. C* **2011**, *115*, 11170.

(21) Kim, H.; Lee, K; Woo,S.I.; Jung, Y; On the mechanism of enhanced oxygen reduction reaction in

nitrogen-doped graphene nanoribbons; *Phys. Chem. Chem. Phys.* **2011**, 13, 17505.

(22) Yu, L.; Pan, X.; Gao, X.; Hu, P.; Bao, X.; Oxygen reduction reaction mechanism on nitrogen-doped graphene: A density functional theory study; *Journal of Catalysis* **2011**, *282*, 183.

(23) Ditchfield, R.; Hehre, W. J.; Pople, J. A.; Self-consistent molecular-orbital methods. IX. an extended Gaussian-type basis for molecular-orbital studies of organic molecules; *J. Chem. Phys.* **1971**, *54*,724.

(24) Hehre, W. J.; Ditchfield, R.; Pople, J. A.; Self-consistent molecular orbital methods. XII. further extensions of Gaussian-type basis sets for use in molecular orbital studies of organic molecules; *J. Chem. Phys.* **1972**, 56, 2257.

(25) Hariharan, P. C.; Pople, J. A.; The influence of polarization functions on molecular orbital hydrogenation energies; *Theor. Chem. Acc.* **1973**, *28*, 213.

(26) Francl, M. M.; Pietro, W. J.; Hehre, W. J.; Binkley, J. S.; DeFrees, D. J.; Pople, J. A.; Gordon, M. S.; Selfconsistent molecular orbital methods. XXIII. a polarization type basis set for second row elements; *J. Chem. Phys.* **1982**, *77*, 3654.

(27) Yeager, E.; Electrocatalysts for O_2 reduction; *Electrochimica Acta* **1984**, *29*, 1527.

(28) Sepa, D. B.; Vojnovic, M. V.; Vracar, L. M.; Damjanovic, A.; Different views regarding the kinetics and mechanisms of oxygen reduction at Pt and Pd electrodes; *Electrochimica Acta* **1987**, *32*, 129.

(29) Sidik, R. A.; Anderson, A. B.; O_2 reduction on graphite and nitrogen-doped graphite: experiment and theory; *J. Phys. Chem. B* **2006**, *110*, 1787.

(30) Roques, J.; Anderson, A. B.; $Pt_3Cr(111)$ alloy effect on the reversible potential of OOH (ads) formation from O_2 (ads) relative to Pt (111)[1]; *J. Fuel Cell Sci. Tech.* **2005**, *2*, 86.

(31) Kurak, K. A.; Anderson, A. B.; Nitrogen-treated graphite and oxygen electroreduction on pyridinic edge sites; *J. Phys. Chem. C* **2009**, *113*, 6730.

(32) Roques, J.; Anderson, A. B.; Electrode potential-dependent stages in OH_{ads} formation on the Pt_3Cr

alloy (111) surface; *J. Electrochem. Soc.* **2004**, *151*, E340.

(33) Walch, S..; Dhanda, A..; Aryanpour, M.; Pitsch, H.; Mechanism of molecular oxygen reduction at the cathode of a PEM fuel cell: Non-electrochemical reactions on catalytic Pt particles; *J. Phys. Chem. C* **2008**, *112*, 8464.

(34) Chen, R. R.; Li, H. X.; Chu, D.; Wang, G. F.; Unraveling oxygen reduction reaction mechanisms on carbon-supported Fe-Phthalocyanine and Co- Phthalocyanine catalysts in alkaline solutions; *J. Phys. Chem.* C **2009**, *113*, 20689.

(35) Feng, T.; Anderson, A. B.; Effective reversible potential, energy loss, and overpotential on platinum fuel cell cathodes; *J. Phys. Chem. C* **2011**, *115*, 4076.

(36) Ruvinskiy, P. S.; Bonnefont, A.; Pham-Huu, C.; Savinova, E. R.; Using ordered carbon nanomaterials for shedding light on the mechanism of the cathodic oxygen reduction reaction; *Langmuir* **2011**,*27*, 9018.

(37) Webster, S.; Maultzsch, J.; Thomsen, C.; Liu, J.; Czerw, R.; Terrones, M.; Adar, F.; John, C.; Whitley, A.; Carroll, D. L.; Raman characterization of nitrogen doped multiwalled carbon nanotubes; *Mater. Res. Soc.* **2003** *772*, M7.8.1.

(38) Soin, N.; Roy, S.; Hazra, K. S.; Misra, D. S.; Lim, T. H.; Hetherington, C. J.; McLaughlin, J. A.; Enhanced and stable field emission from in situ nitrogen-doped few-layered graphene nanoflakes; *J. Phys. Chem. C* **2011**, *115*, 5366.

(39) Huang, S.; Terakura, K.; First-principles calculation of the electronic properties of graphene clusters doped with nitrogen and boron: Analysis of catalytic activity for the oxygen reduction reaction; *Phys. Rev. B* 2009, 80, 235410.

(40) Zhao, L.; He, R.; Rim, K. T.; Schiros, T.; Kim, K. S.; Zhou, H.; Gutierrez, C.; Chockalingam, S. P.; Arguello, C. J.; Palova, L.; Nordlund, D.; Hybertsen, M. S.; Reichman, D. R.; Heinz, T. F.; Kim, H. P.; Pinczuk, A.; Flynn, G. W.; Pasupathy, A. N.; Visualizing individual nitrogen dopants in monolayer

graphene; *Science* **2011**, *333*, 999.

(41) Xiong, W.; Du, F.; Liu, Y.; Perez, A.; Supp, Jr., M.; Ramakrishnan, T.S.; Dai, L.; Jiang, L.; 3-D carbon nanotube structures used as high performance catalyst for oxygen reduction reaction; *J. Am. Chem. Soc.* **2010**, *132*, 15839.

(42) Dai, J.; Yuan, J.; Giannozzi, P.; Gas adsorption on graphene doped with B, N, Al, and S: A theorital study; *Appl. Phys. Lett.* **2009**, *95*, 232105.

(43) Aihara, J.; Reduced HOMO-LUMO gap as an index of kinetic stability for polycyclic aromatic hydrocarbons; *J. Phys. Chem. A* **1999**, 103 7487.

Tables

Table 1. Adsorption energy difference and reversible potentials of each ORR reaction step on the graphene with two doped nitrogen atoms and two Stone-Wales defects.

Reaction order	Chemical Reaction	Adsorption energy difference ΔE_r (eV)	Reversible potential U^0 (V/SHE) *	Reversible potential U (V/SHE)
1	$O_2+H^++e^-\rightarrow{}^*OOH$	1.170	-0.046	1.120
2	$^*OOH+H^++e^-\rightarrow{}^*OH+OH$	1.150	-0.664	0.480
3	$OH+H^++e^-\rightarrow H_2O$	0.0	2.813	2.813
4	$^*OH+H^++e^-\rightarrow H_2O$	-2.320	2.813	0.493
Overall	$O_2+4H^++4e^-\rightarrow 2H_2O$	0.00	1.229	1.228

* Ref.28.

Table 2. The number of active sites and effective reversible potential for nitrogen-doped graphene.

	The number of N atoms in cluster	**0**	**1**	**2**	**3**	**4**
No defect	The number of active sites	0	1	3	2	1
	Effective Reversible potential V/SHE	-	1.04	1.07~1.15	1.07	1.15
With defect	The number of active sites	0	1	3	2	3
	Effective Reversible potential V/SHE	-	1.04	1.15	1.07~1.15	1.15

Figure Captions

Figure 1. Optimized structure of each electron transformation in oxygen reduction reaction: (a) Initial position of OOH from nitrogen doped graphene, (b) OOH adsorbs on the graphene, (c) O-O bond is broken, (d) One water molecule is generated, and (e) C-O bond is broken, the second water molecule is generated. Grey, blue, read and small white balls represent carbon, nitrogen, oxygen and hydrogen atoms, respectively.

Figure 2. (a) Atomic charge density and (b) Spin density distribution on the nitrogen-doped graphene with Stone-Wales defects.

Figure 3. The adsorption energy of OOH on graphene as a function of (a) Spin density for atomic charge *e*= -0.087 ~ +0.085, and *e* = +0.205 ~ +0.263, and (b) Atomic charge density for *s*= -0.036 ~ +0.0072.

Figure 4. The graphene structures with a number of dopants and defects. N= the number of nitrogen dopants. Grey, blue, and small white balls represent carbon, nitrogen, and hydrogen atoms, respectively. The structures in the first row contain no defects while the structures in the second row have.

Figure 5. The reversible potentials of ORR versus N cluster size for the graphene (a) without defects, and (b) with defects. Dot lines represent standard reversible potential (1.228 V).

Figure 6. Reaction scheme of ORR on N-graphene in acidic solution, where ❶ presents an intermediate OOH adsorption mechanism and ❷ a direst O_2 adsorption mechanism, and ① ~⑤ represents 5 reaction paths after OOH adsorption.

Figure 7. HOMO-LOMO energy gap as a function of the number of nitrogen doped atoms in cluster with and without Stone-Wales defects.

Figures

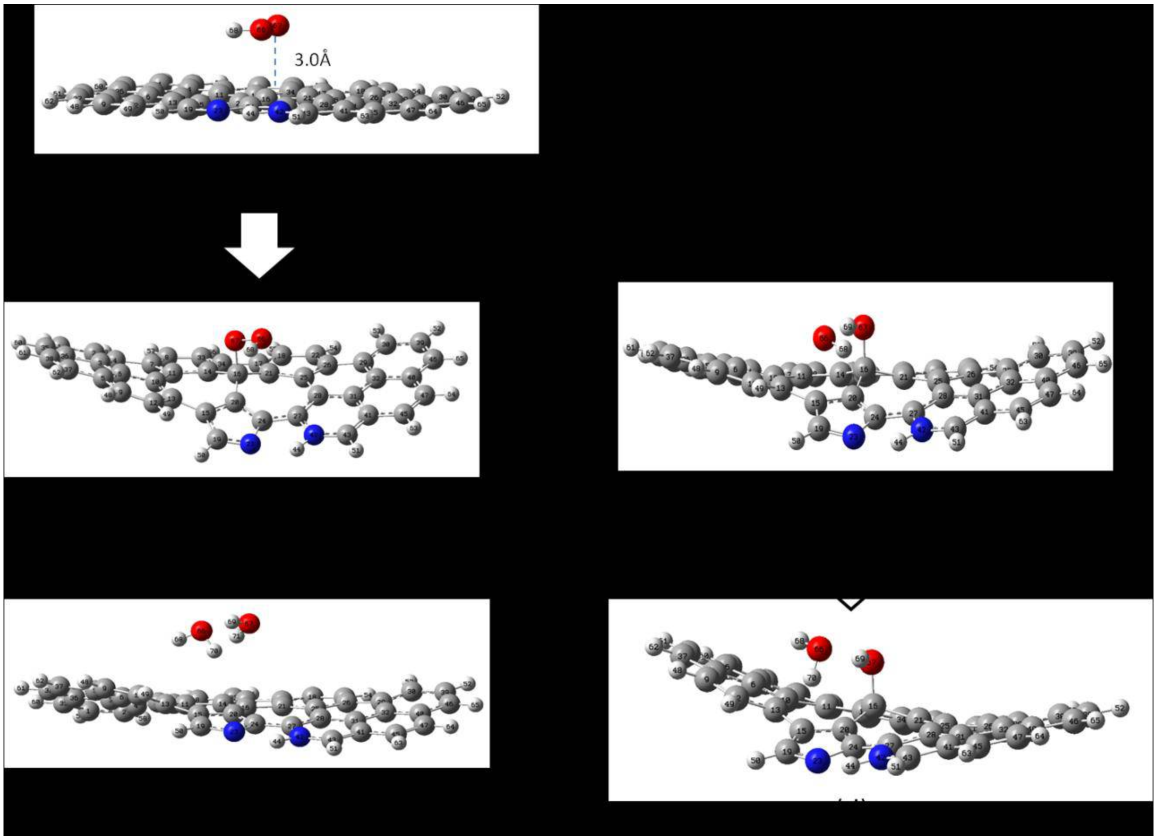

Figure 1.

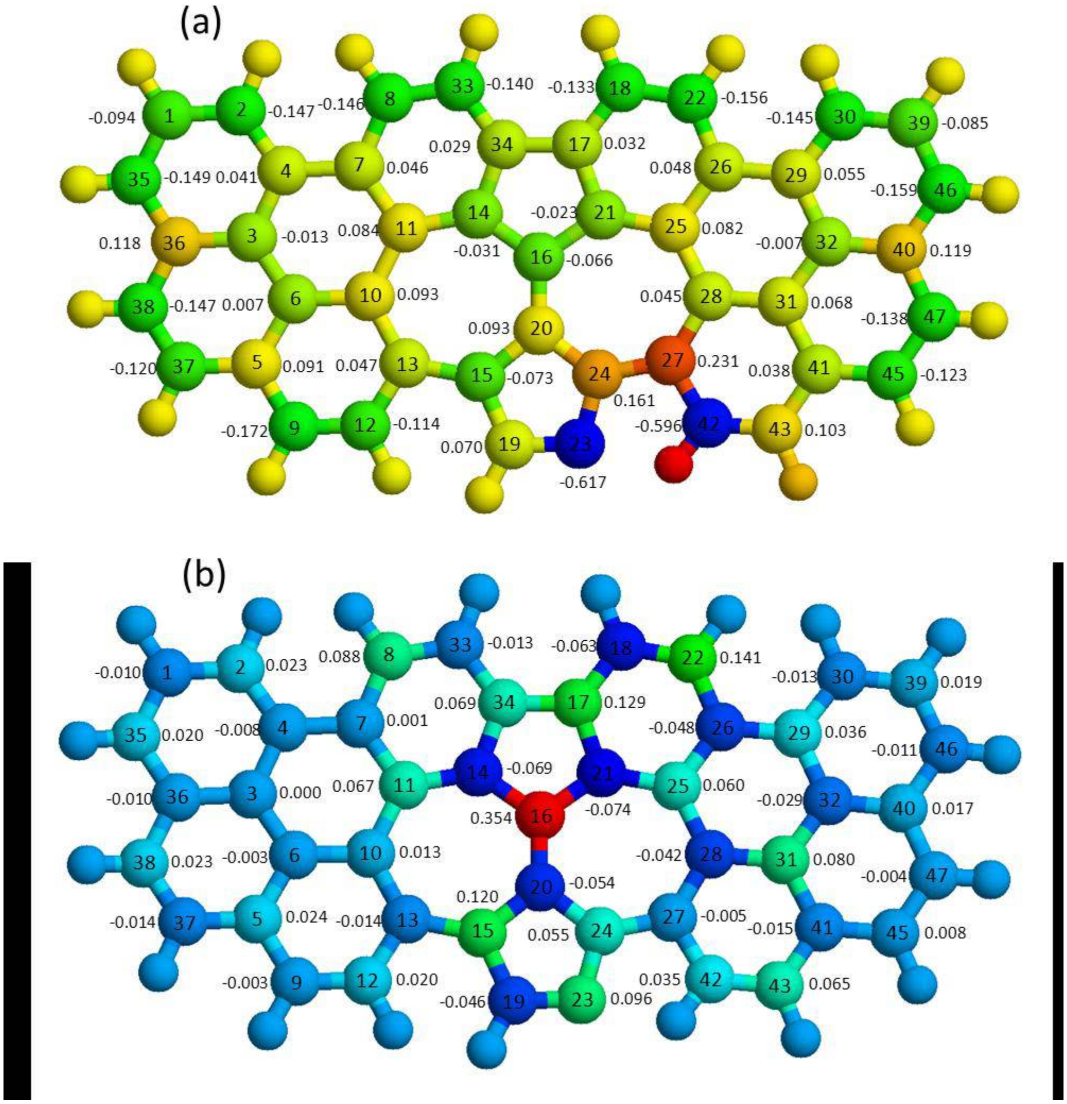
(a)
33 -0.140 -0.133 18 22 -0.156
-0.094 1 2 -0.147 -0.146 8 -0.145 30 39 -0.085
0.029 34 17 0.032
35 -0.149 0.041 4 7 0.046 0.048 26 29 0.055 -0.159 46
14 -0.023 21 25 0.082
0.118 36 3 -0.013 0.084 11 -0.031 -0.007 32 40 0.119
16 -0.066
38 -0.147 0.007 6 10 0.093 0.045 28 31 0.068 -0.138 47
0.093 20
-0.120 37 5 0.091 0.047 13 15 -0.073 24 27 0.231 0.038 41 45 -0.123
0.161
-0.172 9 12 -0.114 0.070 19 23 -0.596 42 43 0.103
-0.617
(b)
33 -0.013 -0.063 18 22 0.141
-0.010 1 2 0.023 0.088 8 -0.013 30 39 0.019
0.069 34 17 0.129
35 0.020 -0.008 4 7 0.001 -0.048 26 29 0.036 -0.011 46
0.067 11 14 -0.069 21 25 0.060
-0.010 36 3 0.000 0.354 16 -0.074 -0.029 32 40 0.017
38 0.023 -0.003 6 10 0.013 -0.042 28 31 0.080 -0.004 47
0.120 20 -0.054
-0.014 37 5 0.024 -0.014 13 15 0.055 24 27 -0.005 -0.015 41 45 0.008
-0.003 9 12 0.020 0.035 42 43 0.065
-0.046 19 23 0.096

Figure 2.

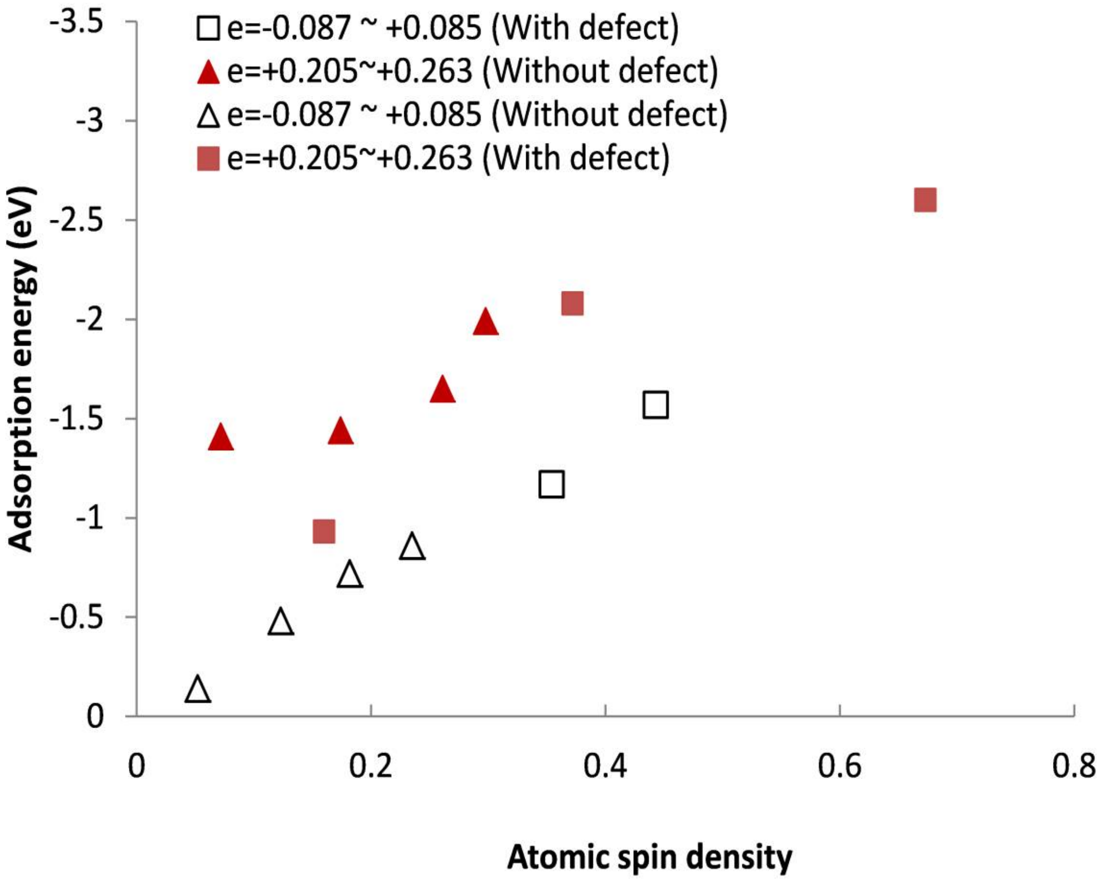
□ e=-0.087 ~ +0.085 (With defect)
▲ e=+0.205~+0.263 (Without defect)
△ e=-0.087 ~ +0.085 (Without defect)
■ e=+0.205~+0.263 (With defect)
Adsorption energy (eV)
-3.5
-3
-2.5
-2
-1.5
-1
-0.5
0
0
0.2
0.4
0.6
0.8
Atomic spin density

(a)

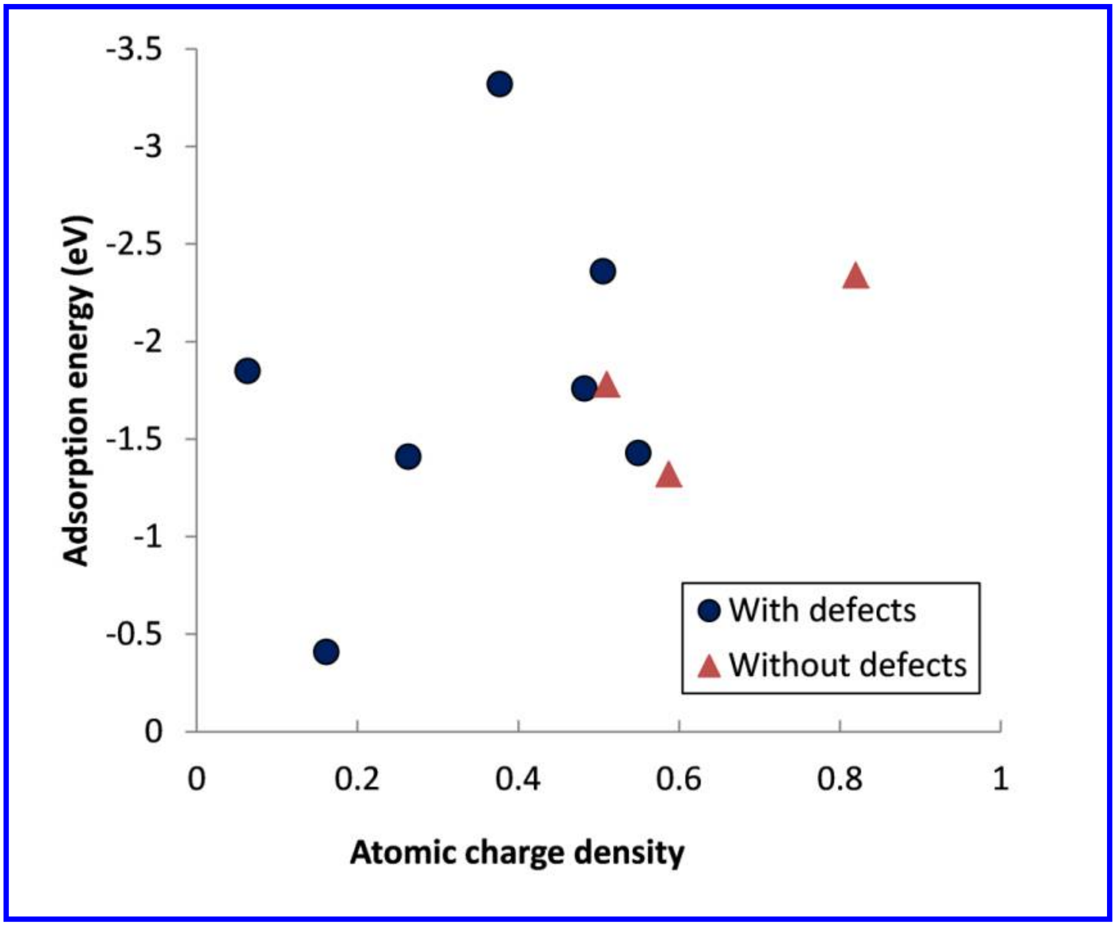
-3.5
-3
-2.5
-2
-1.5
-1
-0.5
0
Adsorption energy (eV)
0
0.2
0.4
0.6
0.8
1
Atomic charge density
● With defects
▲ Without defects

(b)

Figure 3.

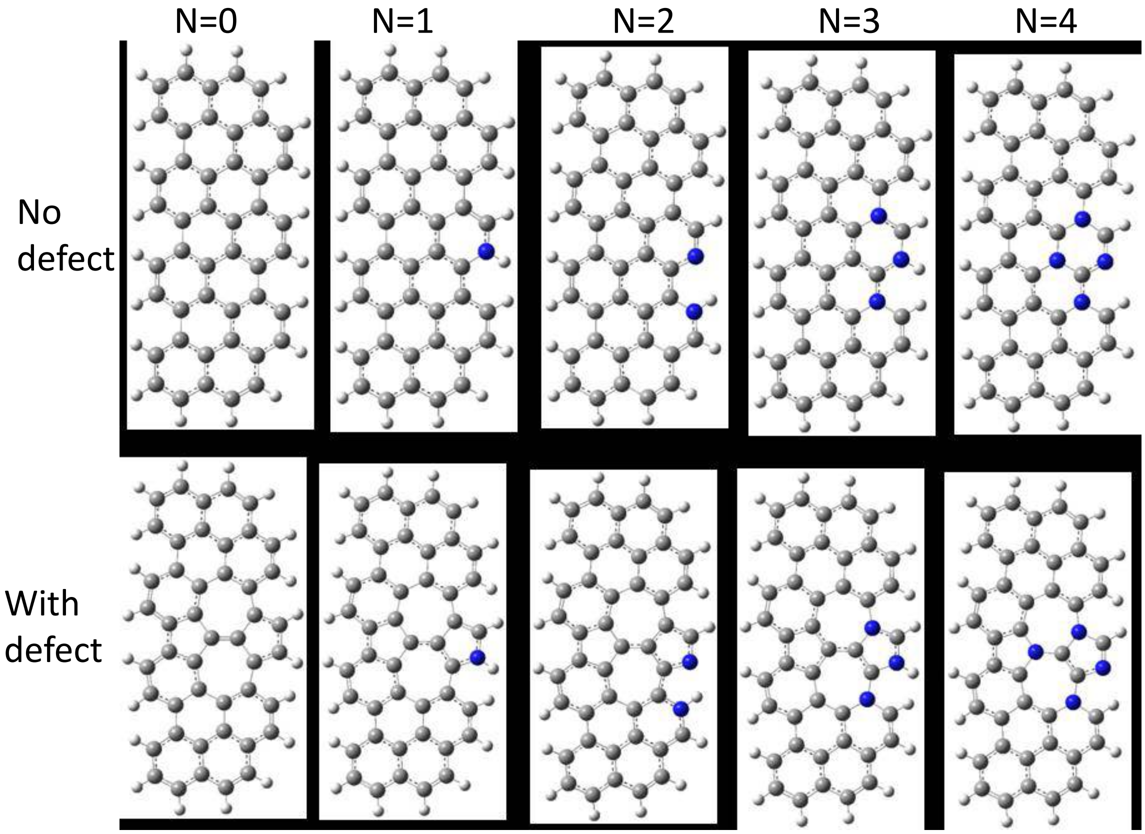

Figure 4.

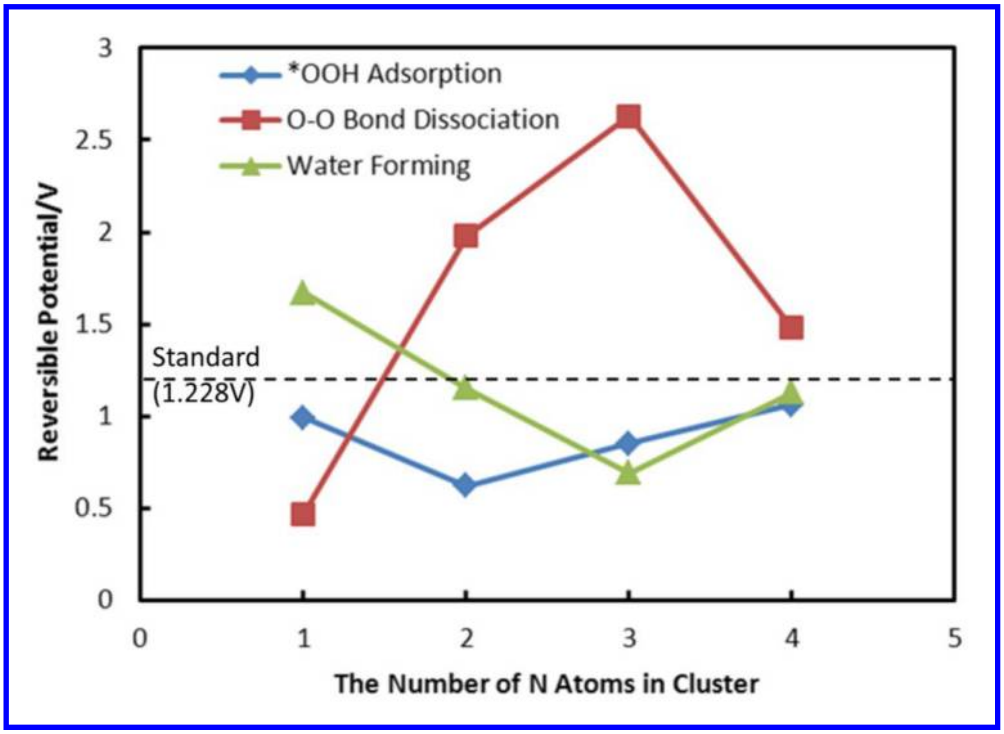
3
2.5
2
1.5
1
0.5
0
Reversible Potential/V
*OOH Adsorption
O-O Bond Dissociation
Water Forming
Standard
(1.228V)
0
1
2
3
4
5
The Number of N Atoms in Cluster

(a)

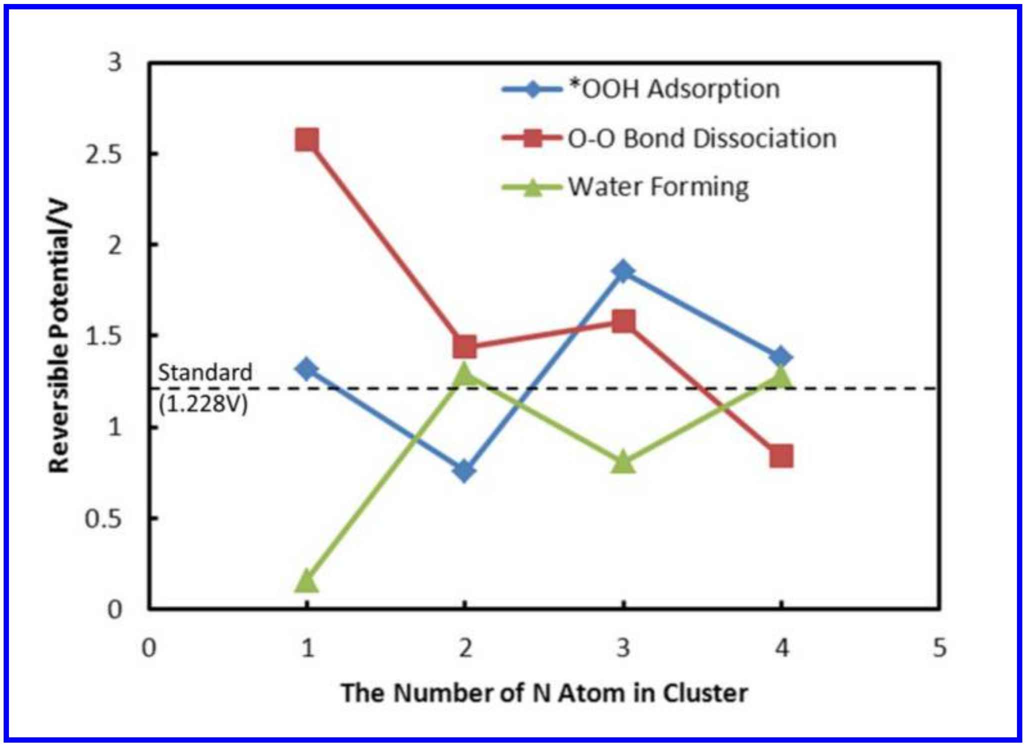
3
2.5
2
1.5
1
0.5
0
Reversible Potential/V
*OOH Adsorption
O-O Bond Dissociation
Water Forming
Standard
(1.228V)
0
1
2
3
4
5
The Number of N Atom in Cluster

(b)

Figure 5.

[redacted]

Figure 6.

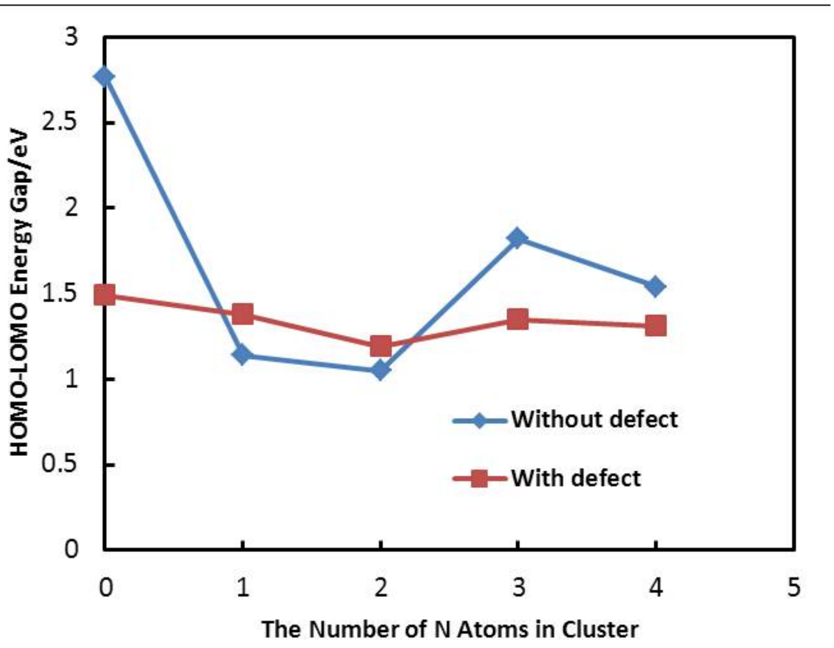

Figure 7.

Table of Contents (TOC) Image